Proceedings of the ASME 2025
International Mechanical Engineering Congress and Exposition
IMECE2025
November 16-20, 2025, Memphis, Tennessee

IMECE2025-166954

ENABLING ON-DEMAND AEROSPACE COMPONENT MANUFACTURING: APPLYING TOPOLOGY OPTIMIZATION OF GE JET ENGINE BRACKET USING METAL FFF

Abhishek Singh[1], Luohaoran Wang[1], Abdul Sayeed Khan[2,3], Aren Vardhan Pilli[1], Mihaela Banu[1]

[1]Mechanical Engineering Department, University of Michigan Ann Arbor, MI 48109 (USA).

[2]Naval Architecture and Marine Engineering Department, University of Michigan Ann Arbor, MI 48109 (USA).

Current Address: [3]Materials Science and Technology Division, Oak Ridge National Laboratory, TN 37830 (USA).

ABSTRACT

Additive Manufacturing (AM) offers advantages over conventional manufacturing processes, particularly in reducing the number of parts made with multistage combined technologies, which often result in low manufacturing yields or require post-processing. AM facilitates the production of complex geometries with fine features, overhangs, and lattice structures. For instance, Laser Powder Bed Fusion (LPBF) enables the fabrication of intricate parts that can be easily post-processed by removing residual powder. Laser powder bed AM technologies are widely discussed in the literature due to their design freedom of creating complex geometries, with and without need for support generation. However, rapid solidification due to a thermal gradient in the build direction, which leads to the formation of columnar grains and warpage, is one of the challenges. To address this challenge, we propose layer-by-layer metal FFF technology, followed by debinding and sintering process, as an alternative to powder bed approaches. Furthermore, DfAM principles are discussed to minimize the need for support, enable easy post-processing to achieve better surface finish in component design, particularly to meet high tolerances for aerospace and healthcare applications.

In this paper, we explore the current state of the art in design for additive manufacturing (DfAM) for the aerospace industry to develop strategies for simplifying the challenges of fabricating intricate features and complex geometries. This include applying DfAM principles and topology optimization to reduce the weight of the GE engine bracket without compromising part performance in terms of structural rigidity and functionality, covering support assessment, fill density, material selection, and process optimization to improve manufacturability. We have performed topology optimization (TO) on the Jet engine bracket in the SOLIDWORKS 2024 R2 and validated the design under the standard loading conditions for Jet engine. Topology Optimization (TO) is performed in a high-fidelity environment, achieving weight reductions of 44%, 50%, and 60% of the original bracket design, followed by simulations to ensure structural rigidity and preservation of clamping features. The 3D-printed parts from TO on the metal FFF has been evaluated through precision in realizing filling radii (compared with CAD models), accuracy in holes, cavities, dimensional accuracy, and process efficiency.

To conclude, DfAM principles have been successfully applied to the GE engine bracket and validated under the suggested loading conditions, which have enhanced accessibility and manufacturability for the jet engine bracket, achieving a 60% weight reduction from the original design while maintaining its performance, demonstrating the capabilities of metal-FFF technology for aerospace applications.

ABBREVIATIONS

GE	General Electric
FFF	Fused filament fabrication
DFAM	Design for additive manufacturing
FDM	Fused deposition modeling
LPBF	Laser powder bed fusion
TO	Topology optimization
SLM	Selective laser melting
LPBF	Laser powder bed fusion
DED	Direct energy deposition
DMD	Direct metal deposition

Notice: This manuscript has been authored by UT-Battelle, LLC, under contract DE-AC05-00OR22725 with the US Department of Energy (DOE). The US government retains and the publisher, by accepting the article for publication, acknowledges that the US government retains a nonexclusive, paid-up, irrevocable, worldwide license to publish or reproduce the published form of this manuscript, or allow others to do so, for US government purposes. DOE will provide public access to these results of federally sponsored research in accordance with the DOE Public Access Plan (https://www.energy.gov/doe-public-access-plan).

1. INTRODUCTION

Design freedom, customization, and the flexibility and capability to tailor properties specific to applications or users' needs are some of the main highlights of additive manufacturing. AM enables the fabrication of parts as a whole or reduces parts' processing, thereby minimizing the need for post-integration and reducing complexity [1], [2], [3]. With the growth of the AM market, an important aspect, Design for Additive Manufacturing (DfAM), has been widely discussed in recent years [4]. DfAM is a broad term that emerged in practice around the early 2000s, but it is being explored, and its foundational principles started developing around the 1990s with the introduction of rapid prototyping. The DFAM started gaining attention after 2006 with the introduction of metal AM when manufacturability of complex designs made possible by emergence of SLM and EBM technologies. As AM continues to expand, there is a demand for design methodologies to drive innovation and increase accessibility for manufacturing intricate geometries and utilizing various novel materials and AM technologies. Recent advancements include the introduction of novel materials, such as high-strength steels, nickel-based superalloys, titanium, copper, Inconel, and tool steels in the aerospace sector for lightweight applications, which not only reduce the complexity of intricate parts but also offer higher performance [4], [5]. Despite significant advancements, the capabilities of AM have not been fully exploited due to factors such as high capital investment, machine and equipment costs, lack of skilled workforce, longer production times, and insufficient design expertise. A key challenge among these is the need to understand proper design algorithms, referred to as Design for Additive Manufacturing (DfAM).

DfAM is the practice of optimizing the designing of a product together with its production system to reduce its lead time for manufacturing while maintaining its cost-effectiveness and to increase performance, quality, and profitability [4], [6], [7], [8]. It is an approach for selecting suitable materials and processes for specific applications, ensuring digital workflow compatibility through CAD modeling and simulation. DfAM strategies include some specific design rules that require user expertise and interaction with design tools, particularly for optimizing part orientation, preparing the build, and defining assemblies. These strategies aim to consolidate components to minimize part count, reduce the need for support structures, and ensure that the final parts meet performance requirements. This aims to facilitate user-driven DfAM that explores the full design freedom while maintaining part strength and performance. The components of DfAM are briefly outlined in Figure 1. Even with several advancements, studies limit the full exploration to understand the DfAM tools, rules, and methodologies, which is limiting the adoption and impact in the AM industry [9].

FIGURE 1: KEY COMPONENTS OF DESIGN FOR ADDITIVE MANUFACTURING, HIGHLIGHTING THE INTEGRATION OF DESIGN, MATERIAL SELECTION, OPTIMIZATION, WORKFLOW, AND PROCESS SELECTION.

Powder bed AM technologies, for example LPBF, facilitate the manufacturability of parts with overhang features that can be easily post-processed by removing residual powder. Laser powder bed AM technologies are widely discussed in the literature due to their design freedom for creating complex geometries, with or without the need for support generation [10], [11]. However, due to thermal gradients, mainly in the build direction during layer-by-layer sintering, the formation of columnar grains leads to distortion in the parts [12], [13]. In contrast, metal FFF AM has demonstrated reliable manufacturability and the ability to maintain desired performance in parts with low to moderately intricate features, even where support structures are required, provided that DfAM principles are effectively applied. Topology optimization (TO) is one of the supporting DfAM principles employed to reduce material from parts while maintaining their functional performance. TO is a computational, mathematically driven approach for reducing overall weight and optimizing material distribution while maintaining the part's performance for its intended applications. However, this algorithmic approach to optimization often results in irregular and complex part geometries and contours, making them more difficult to manufacture compared to the original design.

In this research, we applied DfAM principles to GE's jet engine bracket and fabricated it using metal FFF to analyze and discuss the manufacturability and complexity of the part in terms of the irregular shapes resulting from topology optimization. We aimed to eliminate unnecessary material from the jet engine component to reduce overall weight while ensuring that the

© 2025 by ASME

strength, durability, and performance of the part were not compromised. Simulation and validation were performed to assess the part's performance under the given loading conditions, details of which are discussed in later sections.

2. MATERIALS AND METHODS

Material selection for aerospace and healthcare applications is crucial, as it plays a significant role in determining the longevity of parts over the course of the application. In terms of application, the materials must withstand the harsh environment, qualify for manufacturing, and possess high strength under the specified loading conditions. Stainless steel is widely used in aerospace applications due to its excellent corrosion resistance and mechanical strength.

In this research, Markforged's 17-4 PH stainless steel (Version v2) is used. This material utilizes an optimized polymer–wax binder-based filament, typically containing over 85% metal powder. The binder composition in the metal powder ensures printability and keep the metal powder bound together during the extrusion and printing process. 17-4 PH stainless steel is selected due to its high impact strength, fracture toughness, and resistance to corrosion [14], [15]. The heat-treated precipitation hardening process enhances the material's performance, particularly in terms of toughness and tensile strength, when compared to conventional stainless steels. Furthermore, its excellent corrosion resistance and good machinability make it well-suited for post-sintering processing to achieve improved surface finish.

TABLE 1: MECHANICAL PROPERTIES OF 17-4 PH STAINLESS STEEL [14], [15]

Property	Value
Elastic Modulus (GPa)	160.00
Poisson's Ratio	0.27
Shear Modulus (GPa)	62.99
Mass Density (kg/m3)	9940.00
Tensile Strength (GPa)	1.16
Yield Strength (GPa)	0.90

Metal additive manufacturing primarily uses processes such as LPBF, SLM, EBM and DMD, which generally require careful powder handling and bed preparation. In metal sintering and direct metal deposition processes, the layer-by-layer laser scanning and rapid solidification cause microstructural columnar grain formation due to the thermal gradient in the build direction. This anisotropy leads to inhomogeneity in the mechanical behavior of the part, which makes the sintering process challenging and requires heat treatment and post-processing to manufacture parts for critical applications in the healthcare and aviation industries [16], [17], [18], [19]. As compared to other metal AM technologies, FFF is quite straightforward and more controllable. In this process, layer lines can be eliminated, and surface smoothness greatly enhanced by wet sanding the green parts before sintering, which reduces post-processing efforts and provides a high-quality surface finish. Also, compared to powder-bed AM technologies, FFF is more convenient and safer, as no powder or bed preparation is involved that could become airborne, making it easier to handle [20], [21].

3. TOPOLOGY OPTIMIZATION AND DESIGN VALIDATION FOR JET ENGINE BRACKET

Topology optimization was performed on a jet engine aircraft bracket using SOLIDWORKS 2024 R2, licensed to the University of Michigan. Aerospace-standard loading conditions were applied to conduct the optimization, based on the GE Jet Engine Bracket design challenge specifications [22]. These conditions are detailed in Figure 2, as stipulated by the challenge guidelines. As per GE's design specifications, the bracket must be specifically designed to endure a maximum static linear load of 35,600 N applied vertically upward, 37,800 N applied horizontally outward, and 42,300 N applied at a 42-degree angle from the vertical. It can withstand a maximum static torsional load of 565 N·m, applied horizontally at the intersection of the pin's centerline and the midpoint between the clevis arms. To proceed with the analysis, the holes of the bracket were constrained as fixed points. For this analysis, we selected stainless steel 17-4 PH as the material, with its properties listed in Table 1.

The main objective of this optimization is to reduce weight as much as possible while ensuring the part remains manufacturable, has minimal irregularities, and maintains structural rigidity and performance under the given loading conditions.

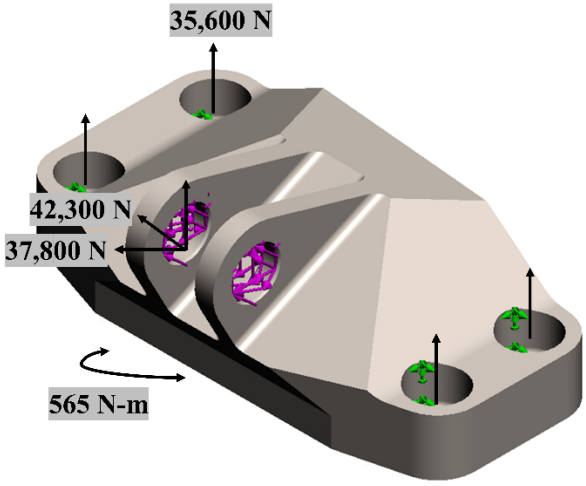

FIGURE 2: STATIC SIMULATION SETUP FOR ENGINE BRACKET IN SOLIDWORKS 2024.

The static simulation was conducted in SOLIDWORKS following the conditions above, using 88,494 solid elements. The initial stress distribution contours are shown in Figure 3. The von Mises stress contours from the initial simulation are shown in Figure 3, which presents different perspectives of the engine bracket to provide a comprehensive view of stress distribution. The figure includes: (a) rear, (b) front, (c) left, (d) right, (e) top,

© 2025 by ASME

and (f) bottom views. This detailed visualization evaluates stress concentrations in different regions of the bracket, helping to identify critical areas where design optimization may be required. The analysis indicates that the maximum von Mises stress reaches 817.1 MPa, shown in red, which is just below the yield strength of 900 MPa, marked by a red arrow on the color scale. This proximity suggests that the design is approaching the threshold of yielding. However, most regions of the component exhibit stress levels within the blue to green range, indicating low to moderate loading across the rest of the structure.

Notably, the clevis pin area, observed from the top left and center views, experiences high stress near the inner surfaces where the pin is inserted. This is typical for shear and bearing stress, highlighting a potential location for local yielding under heavy loading. Additionally, there is a pronounced stress concentration at the curved hole corner, observed from the top center-right view, where the mounting hole intersects the curved geometry. This is likely due to bending or load transmission through the hole and suggests this region is critical under applied loads, especially torsional or combined angled loads.

Furthermore, the bottom face corners, as seen in the bottom center view, also exhibit moderate stress, particularly around the holes where the component might be bolted or mounted. These observations collectively highlight areas that may require reinforcement or modifications to prevent yielding and ensure the structural integrity of the component under operational loads.

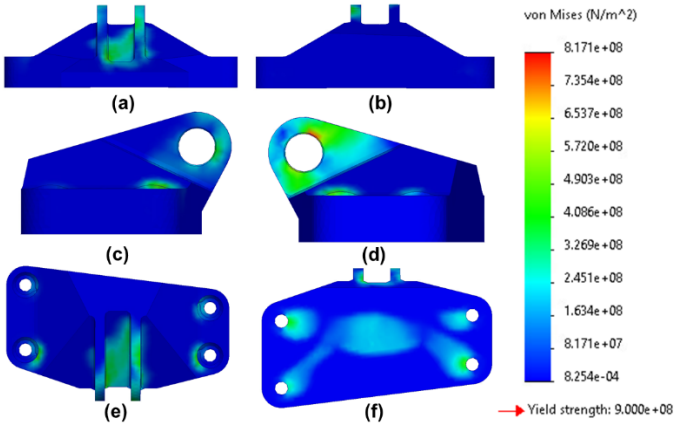

FIGURE 3: VON MISES STRESS CONTOURS FROM THE STATIC SIMULATION OF THE INITIAL ENGINE BRACKET, ILLUSTRATED FROM MULTIPLE PERSPECTIVES: **(a)** REAR, **(b)** FRONT, **(c)** LEFT, **(d)** RIGHT, **(e)** TOP, AND **(f)** BOTTOM VIEW.

After applying the load conditions to the part, the TO process responded by highlighting areas with higher stress concentrations [23]. The regions deemed removable were determined based on the stress distribution, targeting areas with lower stress concentrations for material reduction. The resultant 60% weight reduction is illustrated in Figure 4, showing the areas identified for removal due to their lower stress levels while maintaining the bracket's functional requirements. The holes in the bracket were preserved to ensure that the loading conditions were adequately met.

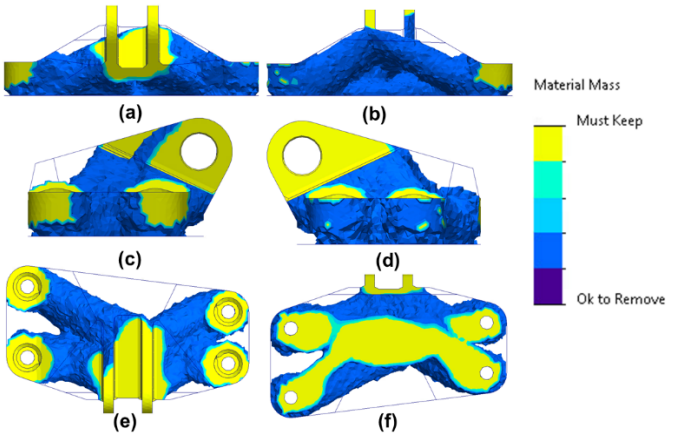

FIGURE 4: REMOVABLE COMPONENT AREA DISTRIBUTION OF THE ENGINE BRACKET, ILLUSTRATED FROM MULTIPLE PERSPECTIVES: **(a)** REAR, **(b)** FRONT, **(c)** LEFT, **(d)** RIGHT, **(e)** TOP, AND **(f)** BOTTOM VIEW.

The static simulation was conducted on the optimized part under the same boundary conditions and the results were shown in Figure 5. Overall, the maximum von Mises stress values from original and TO parts decreased from 817.1 MPa to 700 MPa, and both maximum values remained below the yield strength, indicating acceptable mechanical performance of the component both before and after TO. However, the minimum stress level was significantly lower, starting at 2.52e-2 MPa, compared to the initial part. Following the weight reduction, the load transfer primarily occurred through the component's main structural elements without any load transmission through the bulk material, demonstrating efficient load management in the optimized design.

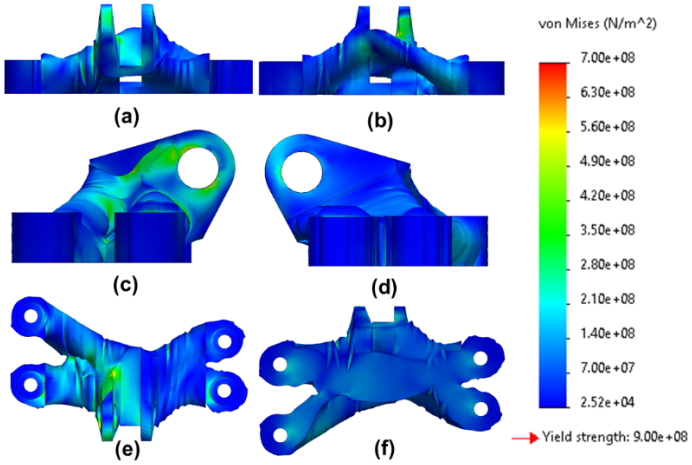

FIGURE 5: VON MISES STRESS CONTOURS FROM THE STATIC SIMULATION OF THE OPTIMIZED ENGINE BRACKET,

© 2025 by ASME

ILLUSTRATED FROM MULTIPLE PERSPECTIVES: **(a)** REAR, **(b)** FRONT, **(c)** LEFT, (d) RIGHT, **(e)** TOP, AND **(f)** BOTTOM VIEW.

4. FUSED FILAMENT FABRICATION ON THE MARKFORGED METAL X 3D PRINTER

We conducted experimental procedures on the Metal X 3D printing system by Markforged™. The fabrication process consists of four stages: - **(i)** *3D printing using metal fused filament fabrication process*, **(ii)** *washing & debinding*, **(iii)** *drying*, and **(iv)** *sintering*. We fabricated four samples: one using the original bracket geometry and three others using geometries optimized through topology optimization, reducing weight by 44%, 50%, and 60%, respectively.

The topology-optimized model was initially exported as an STL file, which is not directly compatible with finite element simulation. To enable mechanical analysis under the same loading conditions, we reconstructed the geometry using a slicing approach with 5 mm increments to approximate the optimized structure. Once the CAD models for all designs were finalized following topology optimization (TO) and validation under the defined loading conditions, they were converted to .STL files and imported into Markforged's Eiger software for pre-processing. The build preparation included the original (non-optimized) part and the topology-optimized designs with 44%, 50%, and 60% weight reductions, as shown in Figure 6. The objective is to ensure manufacturability by analyzing the need for support structures, optimal part orientation, and the requirement for a raft adhesion plate at the base. During pre-processing in Eiger, a solid fill pattern was selected with a layer height of 0.127 mm and four wall layers, resulting in a post-sintered wall thickness of 1.02 mm. The parts are scaled to 120% to account for shrinkage, with the Eiger software automatically applying the scaling to ensure uniform shrinkage during sintering and achieve the intended dimensions. Given the sintering chamber volume restriction, the parts were reduced to 40% scale and printed using the Markforged's Metal X FFF system with 17-4 PH Stainless Steel v2 filament. To ensure easy removal, the parts were printed on the Metal X print sheet to avoid direct contact between the green parts and the build plate. Also, to facilitate smooth flow and extrusion of filament, metal X 3D printer chamber maintain a heated chamber ~ 50 °C, which ensure the powder-binder mixture of the 17-PH stainless steel remain pliable during the printing process.

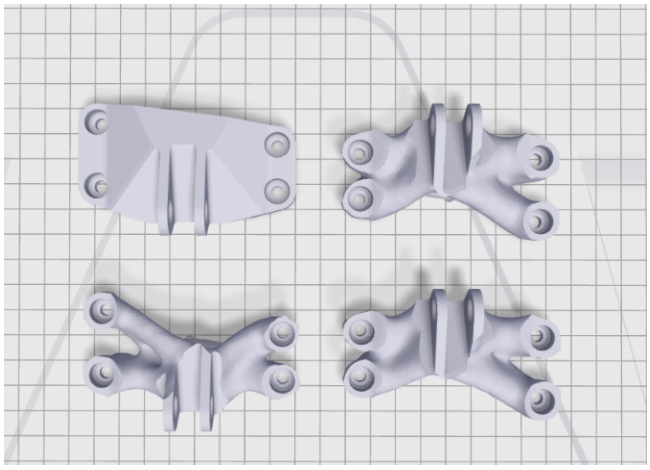

FIGURE 6: BUILD SETUP IN MARKFORGED'S EIGER PLATFORM FOR SUPPORT GENERATION ANALYSIS AND PRE-PROCESSING FOR METAL FFF.

Once the parts were printed, the support structures were carefully removed to minimize post-processing difficulties, and the surfaces were sanded and gently polished. Following this, the debinding process was initiated. The wax binder was removed in two stages: **(i)** washing and **(ii)** sintering. The final finished green parts were weighed, and their initial weights were recorded before being transferred to Markforged's WASH-1 system for washing and debinding as shown in Figure 7. During this process, OPTEON SF 79 solvent degreaser was used to dissolve the binder material. The washing and debinding cycles were performed for the recommended durations specified during build preparation in the Eiger pre-processing software, and the parts were fully dried before sintering.

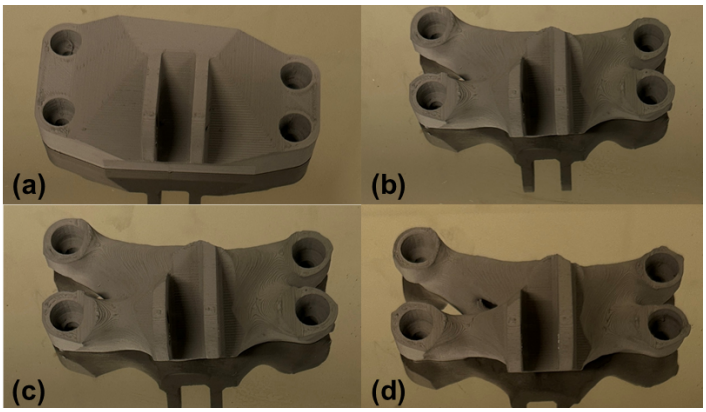

FIGURE 7: 3D PRINTED BRACKET SAMPLES (GREEN PARTS) **(a)** ORIGINAL DESIGN WITHOUT TOPOLOGY OPTIMIZATION (TO), **(b)** TO WITH 44% WEIGHT REDUCTION, **(c)** TO WITH 50% WEIGHT REDUCTION, AND **(d)** TO WITH 60% WEIGHT REDUCTION.

Once the parts were fully dried, referred to as the *brown parts*, their weights were compared to the initial weights of green parts to assess the completeness of binder removal, indicated by

© 2025 by ASME

the corresponding weight loss. The parts were considered properly washed and dried to ensure they met the Markforged-recommended threshold of 3.9% weight reduction for 17-4 PH Stainless Steel V2 material. The final qualified weight loss was recorded, as shown in Figure 8.

$$Weight\ loss\ \% = \frac{\text{Wt. of green part} - \text{Wt. of washed \& dried part}}{\text{Wt. of green part}} \times 100$$

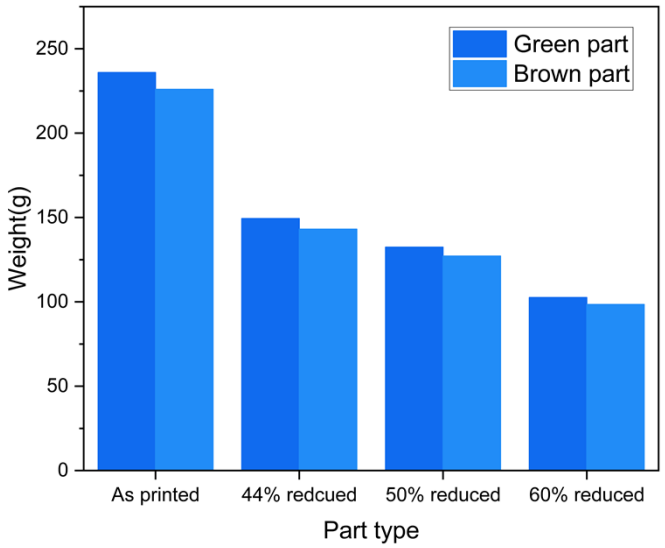

FIGURE 8: COMPARISON OF GREEN AND BROWN (WASHED–DRIED) PART WEIGHTS FOR THE ORIGINAL AND TOPOLOGY-OPTIMIZED DESIGNS (44%, 50%, AND 60% REDUCTIONS), CONFIRMING THE MARKFORGED 3.9% WEIGHT LOSS THRESHOLD.

In the final stage, the parts were placed on a ceramic plate and sintered in the SINTER-1 system. Markforged's Sinter-1 type furnace typically takes ~27 hours for a complete sintering cycle, which utilizes an argon or mixed argon and hydrogen environment to prevent oxidation, reducing the surface of residual oxides on metal particles. It is a multi-stage thermal cycle process, in which the cycle begins with a slow ramp temperature range from 200–600 °C for around 6 hours, which melts and evaporates the wax and thermally decomposes the polymers of the residual binders after the chemical wash debinding process. This slow and controlled ramp prevents cracking in the brown parts. Next, the temperature gradually reaches ~1300-1350 °C to promote solid-state diffusion just below the melting temperature, allowing part densification and bonding of powder particles, turning them into a dense metal part. The shrinkage percentage observed in the parts after sintering is approximately 20%, which was accounted for during pre-processing in the Eiger software.

After sintering, the furnace was allowed to gradually cool to room temperature with the parts inside to prevent thermal shock. Once cooled, the sintered parts were carefully removed from the chamber for inspection and post-sintering evaluation.

5. RESULTS AND DISCUSSION

Topology optimization was performed on the GE jet engine bracket to explore material reduction targets of 44%, 50%, and 60%. The original static simulation results indicated that the maximum stress concentration occurred around the clevis pin area but remained below the yield strength. Simulation results indicated that, even after significant weight reductions, the maximum von Mises stress remained below the material's yield strength of 900 MPa. For instance, the optimized design with 60% weight reduction showed a maximum stress of ~700 MPa, compared to 817.1 MPa in the original design, ensuring the part's structural integrity under the specified loading conditions.

Additionally, a sizable region of the bracket did not efficiently transfer load, with overall stress concentrations being less than 1e12 times the initial stress levels. After optimizing for a 60% weight reduction, the maximum von Mises stress remained below the yield strength, indicating that no failure occurred. An attempt to achieve a 70% weight reduction was made; however, it was unsuccessful due to missing features and formation of irregular contours, which made the design unfeasible for fabrication.

The brackets without topology optimization as shown in figure 9, highlighting smooth surfaces and clean dimensional accuracy, forming a baseline for comparison. Figures 10, 11, & 12 present the post-sintered brackets with 44%, 50% and 60% reduced weight corresponding to each topology optimization level.

Experimentally, the optimized designs were fabricated using the Metal FFF process on the Markforged Metal X system and scaled to 40% of the original size due to sintering chamber constraints. Post-sintered weight measurements closely aligned with the simulated reduction targets as shown in figure 13:

- 44% TO part weighed 138.23 g (39.08% reduction),
- 50% TO part weighed 122.39 g (46.06% reduction),
- 60% TO part weighed 93.73 g (58.69% reduction),
- compared to the 226.90 g of the original part.

© 2025 by ASME

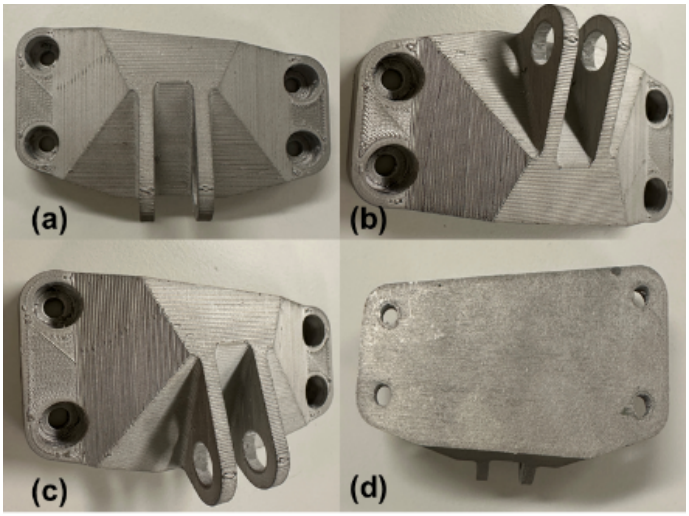

FIGURE 9: POST-SINTERED BRACKET WITHOUT TOPOLOGY OPTIMIZATION, SHOWING **(a)** TOP, **(b)** SIDE-TOP, **(c)** FRONT, AND **(d)** BOTTOM VIEWS WITH SMOOTH SURFACE FINISH AND HIGH DIMENSIONAL ACCURACY IN THE ABSENCE OF COMPLEX GEOMETRICAL REDUCTIONS.

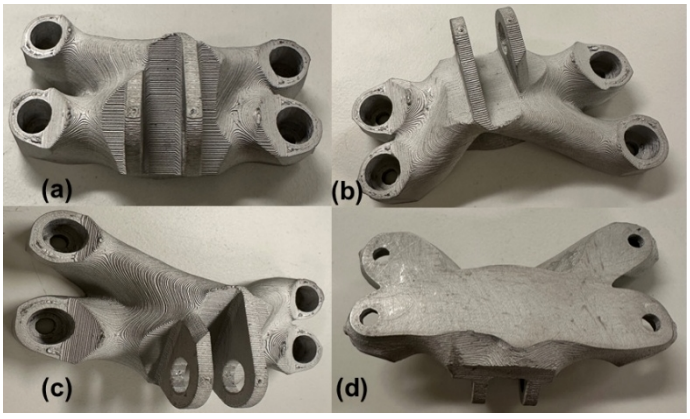

FIGURE 10: POST-SINTERED BRACKET WITH 44% TOPOLOGY OPTIMIZATION, SHOWING **(a)** TOP, **(b)** SIDE-TOP, **(c)** FRONT, AND **(d)** BOTTOM VIEWS.

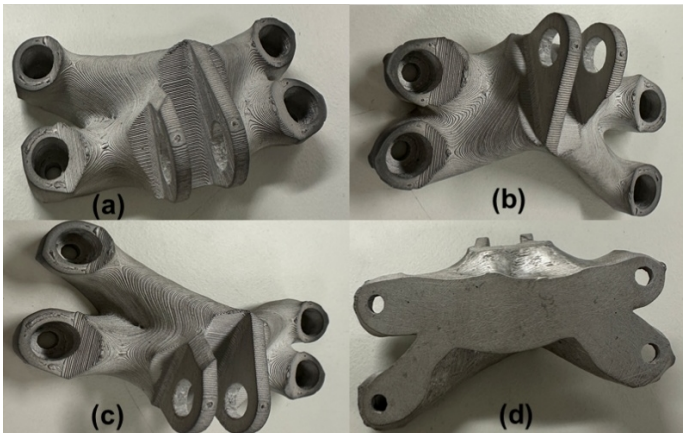

FIGURE 11: POST-SINTERED BRACKET WITH 50% TOPOLOGY OPTIMIZATION, SHOWING **(a)** TOP, **(b)** SIDE-TOP, **(c)** FRONT, AND **(d)** BOTTOM VIEWS.

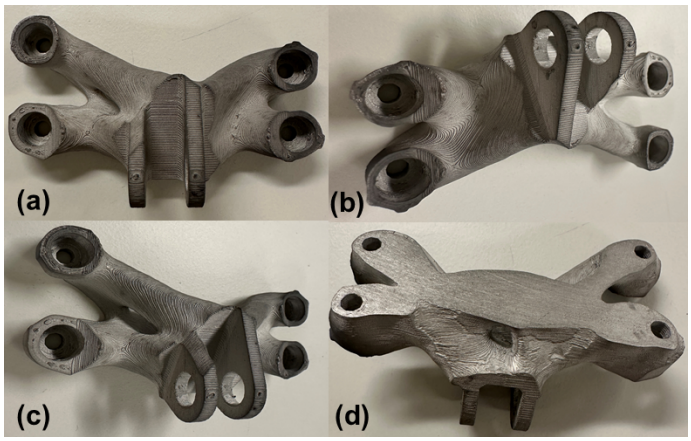

FIGURE 12: POST-SINTERED BRACKET WITH 60% TOPOLOGY OPTIMIZATION, SHOWING **(a)** TOP, **(b)** SIDE-TOP, **(c)** FRONT, AND **(d)** BOTTOM VIEWS.

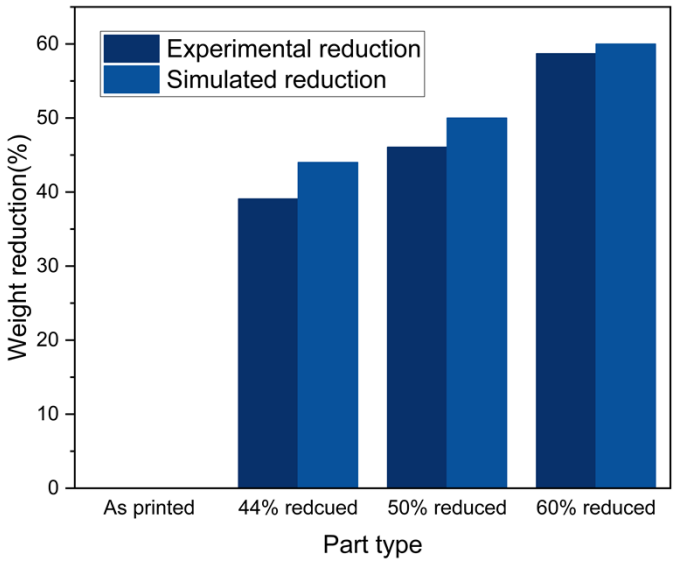

FIGURE 13: POST-SINTERED WEIGHT MEASUREMENTS OF BRACKET **(a)** ORIGINAL DESIGN – 226.90 G, **(b)** 44% TO – 138.23 g., **(c)** 50% TO – 122.39 g., AND **(d)** 60% TO – 93.73 g., CONFIRMING EFFECTIVE MATERIAL REDUCTION THROUGH TOPOLOGY OPTIMIZATION.

To better understand the dimensional accuracy of the manufactured parts on the metal FFF, we primarily focused on the circularity and accuracy of the clamping features: through diameter of the upper and lower clamp holes, and the diameter of the clevis to assess the dimensional accuracy and deviation in the part, and it came out to be very close to the CAD dimensions with error less than 0.5%. The figure below shows the image comparing the dimensions of the features, comparing, as printed, TO with 44% reduced weight, 50% reduced weight, and 60%

© 2025 by ASME

reduced weight. The circularity of the brackets was assessed using a three-point circle and shown to be very uniform, which demonstrates the uniform shrinkages in the brackets.

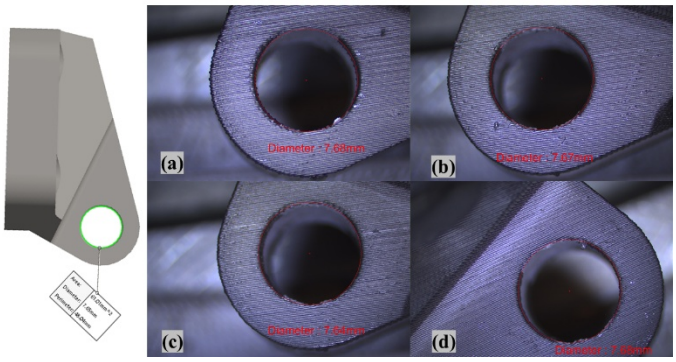

FIGURE 13: FIGURE 13: POST-SINTERED BRACKETS, SHOWING CIRCULARITY MEASUREMENTS OF THE CLEVIS HOLE FOR **(a)** ORIGINAL DESIGN, **(b)** 44% **(c)** 50% AND **(d)** 60% TO WEIGHT REDUCED, DEMONSTRATING CONSISTENT SHRINKAGE AND HIGH CIRCULARITY UNIFORMITY ACROSS ALL DESIGNS.

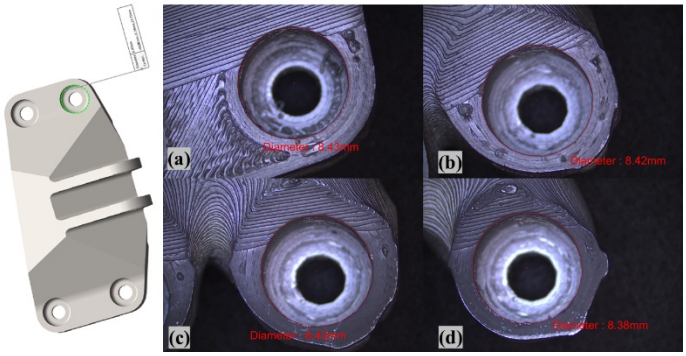

FIGURE 14: POST-SINTERED BRACKETS, SHOWING HOLE DIAMETER MEASUREMENTS OF THE UPPER MOUNTING FEATURE FOR (a) ORIGINAL DESIGN, (b) 44%, (c) 50%, AND (d) 60% TO WEIGHT REDUCED, DEMONSTRATING UNIFORM SHRINKAGE AND HIGH GEOMETRIC FIDELITY ACROSS DESIGNS.

6. CONCLUSION

This study successfully applied DfAM and topology optimization to reduce the weight of a GE jet engine bracket by up to 60% using metal FFF. Even with a 60% aggressive weight reduction, the printed part maintained dimensional accuracy with minimal issues in the overhang regions. Simulation results confirmed that the maximum von Mises stress distribution remained below the yield strength of the material, thereby maintaining considerable mechanical performance. Stiffness was optimized along the principal loading direction defined in the design scenario and loading conditions.

The experimental results also confirmed the uniform shrinkage of the parts with an error of less than 0.5% percent, manufacturability, and alignment with target weight reductions, demonstrating the potential of metal FFF for lightweight aerospace components.

This research effort has demonstrated that, by applying design for additive manufacturing rules, specifically topology optimization, solid-state bound metal deposition techniques such as metal FFF have shown the potential to manufacture geometrically complex, load-bearing components.

Given the complexity of the printed brackets, standard mechanical testing is not directly applicable. Our future work will focus on addressing this by designing custom jigs and fixtures to clamp the brackets with a pin at the clevis and assess the loading performance under the specified conditions. Additionally, we plan to conduct X-ray computed tomography analysis to quantify internal defects, evaluate shrinkage behavior, and assess dimensional deviations.

ACKNOWLEDGEMENTS

The authors would like to acknowledge General Electric for making the jet engine bracket available in the public domain for research and analysis purposes. We also acknowledge GrabCAD for managing the design challenge materials and information in their repository.

CONFLICT OF COMPETING INTEREST

We, the authors, confirm that we have no known competing interests that could influence this research work.

REFERENCES

[1] H. Ko, S. K. Moon, and J. Hwang, “Design for additive manufacturing in customized products,” *International Journal of Precision Engineering and Manufacturing*, vol. 16, no. 11, pp. 2369–2375, Oct. 2015, doi: 10.1007/S12541-015-0305-9/METRICS.

[2] S. A. M. Tofail, E. P. Koumoulos, A. Bandyopadhyay, S. Bose, L. O’Donoghue, and C. Charitidis, “Additive manufacturing: scientific and technological challenges, market uptake and opportunities,” *Materials Today*, vol. 21, no. 1, pp. 22–37, Jan. 2018, doi: 10.1016/J.MATTOD.2017.07.001.

[3] T. D. Ngo, A. Kashani, G. Imbalzano, K. T. Q. Nguyen, and D. Hui, “Additive manufacturing (3D printing): A review of materials, methods, applications and challenges,” *Compos B Eng*, vol. 143, pp. 172–196, Jun. 2018, doi: 10.1016/J.COMPOSITESB.2018.02.012.

[4] P. F. Egan, “Design for Additive Manufacturing: Recent Innovations and Future Directions,” *Designs 2023, Vol. 7, Page 83*, vol. 7, no. 4, p. 83, Jun. 2023, doi: 10.3390/DESIGNS7040083.

[5] A. Kracke, “Superalloys, the Most Successful Alloy System of Modern Times-Past, Present, and Future”.

[6] R. Ponche, O. Kerbrat, P. Mognol, and J. Y. Hascoet, “A novel methodology of design for Additive

© 2025 by ASME

Manufacturing applied to Additive Laser Manufacturing process," *Robot Comput Integr Manuf*, vol. 30, no. 4, pp. 389–398, Aug. 2014, doi: 10.1016/J.RCIM.2013.12.001.

[7] M. K. Thompson *et al.*, "Design for Additive Manufacturing: Trends, opportunities, considerations, and constraints," *CIRP Annals*, vol. 65, no. 2, pp. 737–760, Jan. 2016, doi: 10.1016/J.CIRP.2016.05.004.

[8] P. Nyamekye, A. Unt, A. Salminen, and H. Piili, "Integration of Simulation Driven DfAM and LCC Analysis for Decision Making in L-PBF," *Metals 2020, Vol. 10, Page 1179*, vol. 10, no. 9, p. 1179, Sep. 2020, doi: 10.3390/MET10091179.

[9] H. I. Medellin-Castillo and J. Zaragoza-Siqueiros, "Design and Manufacturing Strategies for Fused Deposition Modelling in Additive Manufacturing: A Review," *Chinese Journal of Mechanical Engineering (English Edition)*, vol. 32, no. 1, pp. 1–16, Dec. 2019, doi: 10.1186/S10033-019-0368-0/FIGURES/8.

[10] S. Chowdhury *et al.*, "Laser powder bed fusion: a state-of-the-art review of the technology, materials, properties & defects, and numerical modelling," *Journal of Materials Research and Technology*, vol. 20, pp. 2109–2172, Sep. 2022, doi: 10.1016/J.JMRT.2022.07.121.

[11] S. R. Narasimharaju *et al.*, "A comprehensive review on laser powder bed fusion of steels: Processing, microstructure, defects and control methods, mechanical properties, current challenges and future trends," *J Manuf Process*, vol. 75, pp. 375–414, Mar. 2022, doi: 10.1016/J.JMAPRO.2021.12.033.

[12] A. Ullah, M. Shah, Z. Ali, K. Asami, A. Ur Rehman, and C. Emmelmann, "Additive manufacturing of ceramics via the laser powder bed fusion process," *Int J Appl Ceram Technol*, vol. 22, no. 3, p. e15087, May 2025, doi: 10.1111/IJAC.15087.

[13] J. Wang, R. Zhu, Y. Liu, and L. Zhang, "Understanding melt pool characteristics in laser powder bed fusion: An overview of single- and multi-track melt pools for process optimization," *Advanced Powder Materials*, vol. 2, no. 4, p. 100137, Oct. 2023, doi: 10.1016/J.APMATE.2023.100137.

[14] Y. Zhang and A. Roch, "Fused filament fabrication and sintering of 17-4PH stainless steel," *Manuf Lett*, vol. 33, pp. 29–32, Aug. 2022, doi: 10.1016/J.MFGLET.2022.06.004.

[15] "17-4 PH Stainless Steel - Robust Metal 3D Printing Material." Accessed: May 12, 2025. [Online]. Available: https://markforged.com/materials/metals/17-4-ph-stainless-steel

[16] Y. Zhang, S. Bai, M. Riede, E. Garratt, and A. Roch, "A comprehensive study on fused filament fabrication of Ti-6Al-4V structures," *Addit Manuf*, vol. 34, p. 101256, Aug. 2020, doi: 10.1016/J.ADDMA.2020.101256.

[17] L. Y. Chen *et al.*, "Anisotropic response of Ti-6Al-4V alloy fabricated by 3D printing selective laser melting," *Materials Science and Engineering: A*, vol. 682, pp. 389–395, Jan. 2017, doi: 10.1016/J.MSEA.2016.11.061.

[18] A. H. Chern *et al.*, "Build orientation, surface roughness, and scan path influence on the microstructure, mechanical properties, and flexural fatigue behavior of Ti–6Al–4V fabricated by electron beam melting," *Materials Science and Engineering: A*, vol. 772, p. 138740, Jan. 2020, doi: 10.1016/J.MSEA.2019.138740.

[19] Y. Kok *et al.*, "Anisotropy and heterogeneity of microstructure and mechanical properties in metal additive manufacturing: A critical review," *Mater Des*, vol. 139, pp. 565–586, Feb. 2018, doi: 10.1016/J.MATDES.2017.11.021.

[20] N. K. Bankapalli, V. Gupta, P. Saxena, A. Bajpai, C. Lahoda, and J. Polte, "Filament fabrication and subsequent additive manufacturing, debinding, and sintering for extrusion-based metal additive manufacturing and their applications: A review," *Compos B Eng*, vol. 264, p. 110915, Sep. 2023, doi: 10.1016/J.COMPOSITESB.2023.110915.

[21] J. Jacob, D. Pejak Simunec, A. E. Z. Kandjani, A. Trinchi, and A. Sola, "A Review of Fused Filament Fabrication of Metal Parts (Metal FFF): Current Developments and Future Challenges," *Technologies 2024, Vol. 12, Page 267*, vol. 12, no. 12, p. 267, Dec. 2024, doi: 10.3390/TECHNOLOGIES12120267.

[22] "GE jet engine bracket challenge | Engineering & Design Challenges | GrabCAD." Accessed: May 10, 2025. [Online]. Available: https://grabcad.com/challenges/ge-jet-engine-bracket-challenge

[23] C. Le, J. Norato, T. Bruns, C. Ha, and D. Tortorelli, "Stress-based topology optimization for continua," *Structural and Multidisciplinary Optimization*, vol. 41, no. 4, pp. 605–620, Apr. 2010, doi: 10.1007/S00158-009-0440-Y/METRICS.

© 2025 by ASME